

RESEARCH

Open Access



Evaluating an enhanced thermal response test (ETRT) with high groundwater flow

Anna Albers^{1*} , Hagen Steger¹, Roman Zorn² and Philipp Blum¹

*Correspondence:
anna.albers@kit.edu

¹ Institute of Applied Geosciences (AGW), Karlsruhe Institute of Technology (KIT), Kaiserstraße 12, 76131 Karlsruhe, Germany

² European Institute for Energy Research (EIFER), Emmy-Noether-Straße 11, 76131 Karlsruhe, Germany

Abstract

Enhanced thermal response tests (ETRT) enable the evaluation of depth-specific effective thermal conductivities. Groundwater flow can significantly influence the interpretation of ETRT results. Hence, this study aims to critically evaluate an ETRT with high groundwater flow ($>0.2 \text{ m d}^{-1}$). Different approaches in determining the specific heat load of an ETRT are compared. The results show that assuming constant electrical resistance of the heating cable with time can account for an inaccuracy of 12% in the determination of effective thermal conductivities. Adjusting the specific heat loads along the borehole heat exchanger (BHE) depth, the specific heat loads vary within 3%. Applying the infinite line source model (ILS) and Péclet number analysis, a depth-average hydraulic conductivity is estimated to be $3.1 \times 10^{-3} \text{ m s}^{-1}$, thereby, confirming the results of a pumping test of a previous study. For high Darcy velocities ($>0.6 \text{ m d}^{-1}$), the uncertainty is higher due to experimental limitations in ensuring a sufficient temperature increase for the evaluation ($\Delta T > 0.6 \text{ K}$). In these depths, the convergence criterion of $\Delta\lambda_{\text{eff}}/\lambda_{\text{eff}} < 0.05/20 \text{ h}$ for the ILS sequential forward evaluation cannot be achieved. Thus, it can be concluded that time-averaging of the heat load by monitoring voltage and current during ETRT is essential. Therefore, the specific heat load adjustment along the heating cable is recommended. To improve the estimation of depth-specific effective conductivities with high groundwater flow and to reduce the sensitivity towards temperature fluctuations ($\Delta T \sim 0.1 \text{ K}$), measures for applying higher specific heat loads during the ETRT are essential, such as actions against overheating of the cable outside the BHE.

Keywords: Actively heated fibre optic, Borehole heat exchanger (BHE), Distributed temperature sensing (DTS), Effective thermal conductivity, Heating cable, Thermal response test (TRT)

Introduction

For the dimensioning of ground source heat pump (GSHP) systems, knowledge of the thermal properties of the subsurface is crucial. Not only the effective thermal conductivity λ_{eff} of the subsurface but also the consideration of groundwater flow is important, since advection can significantly improve the heat transport and, therefore, the efficiency of borehole heat exchangers (BHE) (Stauffer et al. 2014). The thermal response test (TRT) is an established method to determine in-situ effective thermal conductivities (Spitler and Gehlin 2015). In a conventional TRT, a defined heat load is injected into

or extracted from the ground by circulating the heat transfer fluid of the BHE, and the temperature development is measured at the inlet and outlet of the pipes with temperature probes (Verein Deutscher Ingenieure 2020). Using analytical solutions of the heat source equation, e.g., the infinite line source model (ILS), an integral value of the effective thermal conductivity can be derived (Carslaw and Jaeger 1959; Gehlin 2002; Verein Deutscher Ingenieure 2020). Elevated groundwater flow ($>0.1 \text{ m day}^{-1}$) can influence the interpretation of TRT results (Chiasson et al. 2000; Signorelli et al. 2007). The system adjusts fast to the applied heat disturbance when advection is present and significant. If the ILS is applied, higher values of the effective thermal conductivity λ_{eff} will be evaluated due to the groundwater flow and the results will show sensitivity towards evaluation time (Sanner et al. 2005; Angelotti et al. 2018; Katsura et al. 2006). Other evaluation models such as the moving infinite line source model (MILS) are, therefore, recommended if groundwater flow is present (Diao et al. 2004; Molina-Giraldo et al. 2011; Wagner et al. 2013).

In the last years, the TRT setup was further developed (Wilke et al. 2020; Zhang et al. 2021). One development was the application of optic fibre distributed temperature sensing (DTS) for quasi-continuous temperature profile measurement, the so-called distributed TRT (DTRT) with the advantage of determining depth-specific effective thermal conductivities (Fujii et al. 2006; Acuña 2013). Another development was the use of heating cables as a heat source. With heating cables, a more controlled heat load can be applied to the subsurface with less metrological effort (Raymond et al. 2010). With an enhanced TRT (ETRT) (Wilke et al. 2020), also described as actively heated fibre optic TRT (ATRT) (Zhang et al. 2021), fibre optic cables are used along with heating cables. Thus, the advantages of both implementations are combined. Most ETRT studies were conducted with a hybrid cable, a composite cable of fibre optic and heating cables (Huber 2013; Lehr and Sass 2014; Vieira et al. 2017; Galgaro et al. 2018; Maldaner et al. 2019; Dalla Santa et al. 2022; Hakala et al. 2022; Simon and Bour 2022). Hence, temperature measurement and heating were located at the same location. However, some studies used separate heating cable and fibre optic cable in different shanks of the BHE pipe (Vélez Márquez et al. 2018). Thereby, adding the distance between both cables as an additional parameter of uncertainty. Hakala et al. (2022) used an additional reference fibre optic cable to measure the temperature in the subsurface apart from the elevated temperature at the heating cable.

Applying a TRT, the correct determination of the effective thermal conductivity is proportionally linked to the correct calculation of the applied heat load Q . In an ETRT, the heat load is induced by an electrical shortcut of the conductor material of the heating cable. The electrical resistance of the conductor material depends on temperature (Hacker and Sumeder 2020). During an ETRT, the cable temperature increases when the cable is heated. Thereby, its electrical resistance also changes. If the heat load is calculated with a resistance value that is determined before or at the start of an ETRT, the temperature dependence of the resistance is not considered (Luo et al. 2015). In contrast, other studies accounted for this by logging not only the voltage but also the current during the ETRT and then calculating the average heat load for the entire heating time (Huber 2013; Vélez Márquez et al. 2018; Dalla Santa et al. 2022). Raymond et al. (2010) addressed the problem of temperature-dependent

resistance by calibrating their heating cable in a circulation bath under varying temperatures before use. In some studies, the use of a power controller was recommended ensuring a constant heat load over time (Lehr and Sass 2014; Hakala et al. 2022). For several studies, the determination approach for the heat load was not mentioned specifically (Freifeld et al. 2008; Heske et al. 2011; Riegger et al. 2012; Busmann et al. 2015; Vieira et al. 2017; Galgaro et al. 2018; Zhang et al. 2020). Summarising, no distinction between the different ways to calculate the specific heat load is currently made in the ETRT literature. The overall assumption is that the specific heat load does not vary along the length of the heating cable (Lehr and Sass 2014; Maldaner et al. 2019; Dalla Santa et al. 2022; Hakala et al. 2022). However, as implied by Wilke et al. (2020), during an ETRT the temperature increase in the cable varies along the depth depending on the contact material of the cable (air, unsaturated soil, saturated soil, groundwater influence) and, therefore, its electrical resistance. For the application of soil water content determination, Sayde et al. (2014) addressed this by performing an adjustment of the electrical resistance along the cable length using fibre optic temperature measurements.

Of the TRT studies applying heating cables, only a limited amount is conducted in environments with enhanced groundwater flow. For example, Lehr and Sass (2014) analysed ETRT data from a study site with groundwater velocities of $>0.4 \text{ m d}^{-1}$ in various depths. They used Péclet number analysis to derive Darcy velocities from ILS results. Antelmi et al. (2020) applied the MILS to evaluate temperature data (from wireless probes) at a study site with depth-specific groundwater velocities ranging between 0.001 m d^{-1} and 0.26 m d^{-1} . However, the principle of ETRT is analogously applied in hydrogeology as active distributed temperature sensing (A-DTS) focusing mainly on the determination of groundwater flow velocity (Banks et al. 2014; Read et al. 2014; Coleman et al. 2015; Bense et al. 2016). Instead of a hybrid cable, most often the steel case of the fibre optic cable is used as the heating element (Ciocca et al. 2012; Read et al. 2014; Sayde et al. 2014; Del Val et al. 2021; Simon and Bour 2022). Des Tombe et al. (2019) and Bakker et al. (2015) applied the MILS to evaluate groundwater velocity from their A-DTS results. Del Val et al. (2021) placed the fibre optic cable between the well casing and the aquifer. They analysed the temperature data regarding groundwater flow by separating it into different heating phases. The application of ETRT for the identification of depths with enhanced groundwater flow is promising. However, due to the limited amount of studies, further experience and understanding regarding the experimental issues of ETRT are necessary.

The objective of this study is to critically evaluate an ETRT with high groundwater flow. Hence, the results of a case study in Biberach an der Riß (Germany) are presented. The evaluation of depth-specific effective thermal conductivities is conducted by applying the ILS with iterative forward modelling. Furthermore, the hydraulic conductivity is evaluated with Péclet number analysis and compared to the results applying the MILS as well as to the results of a pumping test. In addition, different methods for specific heat load calculations, which are used in the literature, are compared. Thus, for the first time, the specific heat load during the ETRT is adjusted along the heating cable using the theory of temperature-dependent resistances. The models are critically discussed and their suitability is evaluated. Finally, lessons learned are presented from applying an

ETRT with high groundwater flow. Although mainly site-specific results are discussed, this study provides useful information for the planning and evaluation of future ETRT.

Materials and methods

Experiment

Study site

The study site is located at the Biberach University of Applied Sciences in Biberach an der Riß, Germany (Fig. 1a). This area is part of the Molasse basin. The borehole has a depth of 24 m below ground level (bgl) and penetrates the entire upper quaternary aquifer, which is characterised by alternating gravel and sand layers (Fig. 1). The thermal conductivities were measured in the laboratory from bucket samples collected during drilling (Reuß et al. 2012). They were measured with the hot wire method (Isomet 2104, Applied Precision Ltd.) and range between 1.5 and 2.8 W m⁻¹ K⁻¹ (Reuß et al. 2012). Table 1 gives a summary of the thermal conductivity values. In a previous study, the unconfined groundwater level was identified at a depth of about 5.6 m bgl (Reuß et al. 2012). The hydraulic gradient was measured to be $i=0.002$ (Reuß et al. 2012). The mean hydraulic conductivity of the aquifer was measured by a pumping test to be

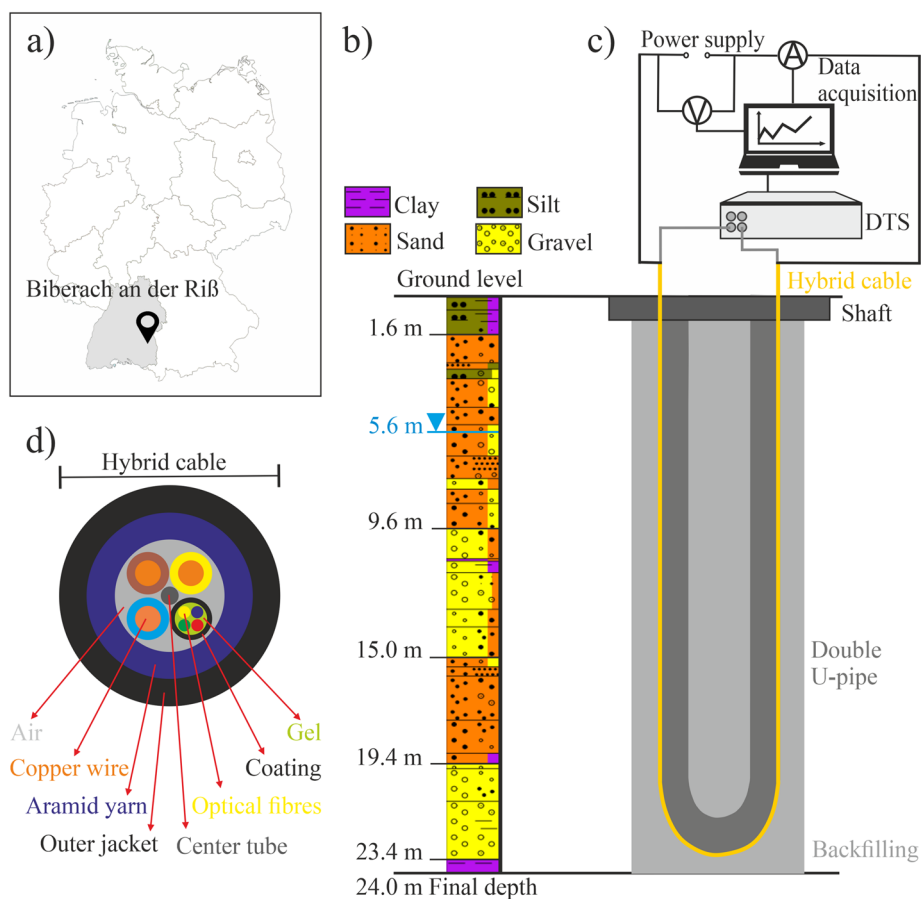


Fig. 1 a Site location in Biberach an der Riß (Germany), b geological profile, c setup of the enhanced thermal response test (ETRT) and d cross section of the hybrid cable

Table 1 Thermal conductivities λ of bucket samples from the drilling at the study site in Biberach an der Riß

Sampling depth z [m bgl]	Thermal conductivity λ [$\text{W m}^{-1} \text{K}^{-1}$]
0.54–1.57	1.9±0.2
1.57–2.74	1.5±0.1
2.74–3.00	2.2±0.1
3.00–3.40	2.4±0.1
3.40–4.61	2.5±0.1
4.61–5.33	2.1±0.1
4.61–5.33	2.7±0.1
5.33–6.62	2.7±0.1
6.62–7.56	2.5±0.1
7.56–8.00	2.3±0.1
8.00–8.60	2.6±0.1
8.60–9.64	2.9±0.1
9.64–10.91	2.5±0.1
11.00–11.48	2.8±0.1
11.48–13.00	2.7±0.1
13.00–13.75	2.8±0.1
13.75–15.00	2.8±0.1
15.00–15.41	2.6±0.1
15.41–15.78	2.3±0.1
15.78–17.63	2.7±0.1
17.63–19.00	2.4±0.1
19.00–19.43	2.5±0.1
19.43–19.64	2.5±0.1
19.64–21.00	2.6±0.1
21.00–23.43	2.6±0.1
Average	2.5±0.4

$k = 3.1 \times 10^{-3} \text{ m s}^{-1}$ (Reuß et al. 2012). From 23.4 m bgl, the aquifer is limited by tertiary sediments of the Upper Freshwater Molasse, predominantly marlstones.

Materials

Figure 1b, c presents the experimental setup. The BHE consists of a double U-pipe with a pipe diameter of 0.025 m. The borehole has a radius of 0.089 m and is grouted with an enhanced backfill material (ThermoCem[®] PLUS, HeidelbergCement, $\lambda_{\text{grout}} = 2.0 \text{ W m}^{-1} \text{K}^{-1}$). In addition to 21 resistance temperature sensors (Pt100), the BHE is equipped with a hybrid cable (Fig. 1d) with an optic fibre for temperature measurements and three copper conductors as heating element (Helukom[®] A-DSQ(ZN)B2Y, $1 \times 4 \text{ G } 50/125 + \text{Cu } 3 \times 0.5 \text{ mm}^2$, length = 69.1 m). The measuring technique was pre-assembled at the outside of one U-pipe.

Enhanced thermal response test (ETRT)

The ETRT started on 28th June 2021. The heating time was about 170 h. A constant voltage of about 75 V was applied to the heating cable with a DC-power supply (Power Ten Inc., R86 D-200100; 200V/100A). The voltage and the resulting current were logged

for the entire heating time. The voltage was measured with a multimeter (Ahlborn, ALMEMO[®] 2590, measurement uncertainty ± 0.4 V). The current was indirectly measured by measuring the voltage at a shunt (Ahlborn, ALMEMO[®] 2590, measurement uncertainty ± 0.5 mV). The temperature was measured using DTS (Agilent, AP Sensing, N4386B, dual end measurement, measurement uncertainty manufacturer value ± 0.2 K). The temperature was measured every 60 s over the entire length of the hybrid cable with a spatial resolution of 0.5 m and a measurement interval of 1 m. The calibration of the DTS measurement was conducted by adjusting the offset to the resistance thermometers when determining the undisturbed ground temperature T_0 . At the beginning, from minutes 19 to 46, there was a break in heating. For the effective thermal conductivity evaluation using the ILS model, this is not expected to influence, since the first hours of temperature data are excluded from the analysis.

Evaluation

Calculation of the specific heat load

For the calculation of the heat load, the electrical power P_{el} [W] is assumed to be equal to the heat load Q [W]:

$$P_{el} = Q \quad (1)$$

With Joule's Law, the heat load is calculated as the product of voltage U [V] and current I [A] (Meschede 2015):

$$Q = UI \quad (2)$$

The specific heat load q [W m^{-1}] is then the heat load per meter length l of the heating cable:

$$q = Ql^{-1} \quad (3)$$

To compare different approaches applied in ETRT studies, Eqs. 2 and 3 are calculated with a single measurement at the beginning of the ETRT, therefore, assuming a constant electrical resistance of the heating cable by time. This value is further referred to as $q_{R=\text{fix}}$. In addition, the arithmetic mean of the specific heat load over the entire heating time is calculated to an average specific heat load q_{ave} .

Spatial adjustment of the specific heat load

According to Ohm's Law, the measured current is related to the electrical resistance R [Ω] of the cable. Electrical resistance is dependent on temperature, as stated in Eq. 4 (Meschede 2015). The resistance at a defined temperature R_T is calculated using the temperature difference to a reference temperature T_{20} and the material-specific temperature coefficient of the resistance (TCR) α_{T20} :

$$R_T = R_{T20}(1 + \alpha_{T20}(T - T_{20})) \quad (4)$$

The reference resistance R_{T20} is calculated using the literature value of the resistivity ρ_{T20} and the length l and cross section A of the heating cable (Meschede 2015):

$$R_T = \rho_{T20} l A^{-1} \quad (5)$$

Values for α_{T20} and ρ_{T20} are taken from Kuchling (2014). Applying Ohm's law, the specific heat load can be calculated using the following equation:

$$q = I^2 R_{T20} (1 + \alpha_T (T - T_{20})) l^{-1} \quad (6)$$

The optic fibre provides temperature values averaged over the measuring time of 60 s for every 0.5 m. Considering the heating cable as a serial connection of resistances, it applies $R_{\text{total}} = \sum R_i$ and $I_{\text{total}} = I_i$. Thus, the specific heat load can be individually determined for every length interval of the hybrid cable. The depth-specific heat load is the sum of the specific heat loads applied to both shanks of the U-pipe. Hence, applying the principle of temperature-dependent resistances using the depth-differentiated temperature measurement of the DTS, the specific heat load is spatially adjusted along the heating cable. This value is further referred to as the adjusted specific heat load q_{adj} .

Evaluation of depth-specific effective thermal conductivities

As the hybrid cable is installed in a loop next to an U-pipe of the BHE (Fig. 1d), the temperature data of two corresponding length intervals of the DTS cable are averaged for each depth interval. In a preliminary data processing step, a moving average of every 20 measurement values of the fibre optic data is applied to reduce the noise. Then, the effective thermal conductivity λ_{eff} is evaluated using the ILS model as given in Eqs. 7 and 8 (Carslaw and Jaeger 1959; Gehlin 2002):

$$T(r, t) - T_0 = \frac{q}{4\pi\lambda_{\text{eff}}} E_i \left[\frac{r_b^2}{4\alpha t} \right] + qR_{\text{th}} \approx \frac{q}{4\pi\lambda_{\text{eff}}} \left(\ln \left(\frac{4\alpha t}{r_b^2} \right) - \gamma \right) + qR_{\text{th}} \quad (7)$$

$$\lambda_{\text{eff}} = \frac{q}{4\pi m}; m = \frac{\Delta T}{\Delta \ln(t)} \quad (8)$$

$T(r, t)$ is the temperature at a defined distance r from the heat source and a specific time t . T_0 is the undisturbed subsurface temperature at time $t=0$. E_i is the exponential integral, α is the thermal diffusivity calculated:

$$\alpha = \frac{\lambda_{\text{eff}}}{\rho c_p} \quad (9)$$

and assuming a volumetric heat capacity of the subsurface ρc_p of $2.5 \text{ MJ m}^{-1} \text{ K}^{-1}$ (Verein Deutscher Ingenieure 2010), r_b is the borehole radius, R_{th} is the thermal borehole resistance, γ is Euler's constant and m is the slope of the linear regression line. The evaluation time is determined by applying the following theoretical starting criterion (Gehlin 2002):

$$t_{\text{start}} = \frac{Pr_b^2}{\alpha} \quad (10)$$

A model error of 5% is accepted by setting $P=10$. Based on the German technical guideline VDI 4640-5 (Verein Deutscher Ingenieure 2020), the data are evaluated iteratively with the sequential forward evaluation. The convergence criterion for

an effective thermal conductivity constancy of $\Delta\lambda_{\text{eff}}/\lambda_{\text{eff}} < 0.05/20$ h is applied. For q , the values for the different specific heat load calculations are inserted into Eq. 8 (see Sects. "Calculation of the specific heat load" and "Spatial adjustment of the specific heat load"). The ILS is only valid for transient heat transport. For the ideal case of constant unique groundwater flow with equal groundwater temperatures, the temperature approaches a constant value at steady-state conditions. If advection is present and significant, these conditions can occur during a TRT. Thus, for the evaluation of effective thermal conductivities, the data are evaluated up to the time when the temperature increase starts to stagnate. Thus, the point, when the effective thermal conductivity starts to approach infinity, is identified. The degree of determination R^2 and the convergence criterion are additionally considered. Measurement uncertainties of the results are considered according to the study by Witte (2013).

Evaluation of hydraulic conductivities with Péclet number analysis

As a simple way to estimate Darcy velocities from TRT results, some studies applied the Péclet analysis (Lehr and Sass 2014; Pambou et al. 2019). This method assumes a simple linear relationship between the advective heat flow component and the difference between effective thermal conductivity λ_{eff} and thermal conductivity by conduction only λ , as stated in Eqs. 11 and 12. Péclet number analysis is applied for depth intervals below the groundwater level of 5.6 m:

$$Pe = \frac{\lambda_{\text{eff}}}{\lambda} - 1 \quad (11)$$

The thermal conductivity λ is taken from laboratory measurements (Sect. "Calculation of the specific heat load"). To attribute the laboratory values to the depth intervals evaluated with DTS, weighted arithmetic mean values of corresponding thermal conductivities are calculated.

$$v_f = \frac{\lambda_{\text{eff}} - \lambda}{l_c \rho c_{p,w}} \quad (12)$$

v_f is the Darcy velocity, $l_c = r_b$ is the characteristic length based on similar studies (Ferguson 2015) and $\rho c_{p,w}$ is the volumetric heat capacity of water.

Assuming a constant hydraulic gradient of $i = 0.002$ (see Sect. "Calculation of the specific heat load"), a value for the hydraulic conductivity k can be derived:

$$k = \frac{v_f}{i} \quad (13)$$

Evaluation of hydraulic conductivities with the MILS

With significant groundwater flow, the evaluation of TRT with the MILS is recommended (Diao et al. 2004; Molina-Giraldo et al. 2011; Wagner et al. 2013). Hence, the data set is additionally evaluated by applying the following MILS (Eq. 14):

$$T_r(r, \vartheta, t) - T_0 = \frac{q}{4\pi\lambda} \exp\left[\frac{v_{th}r\cos(\vartheta)}{2\alpha}\right] \times \int_{\frac{r^2}{4\alpha t}}^{\infty} \exp\left[-\frac{v_{th}^2 r^2}{16\alpha^2 u} - u\right] \frac{du}{u} + qR_{th} \tag{14}$$

ϑ is the angle to the groundwater flow direction. Considering the observation point r as the borehole radius r_b , the average temperature at the borehole wall is calculated as the integral average in all spatial directions (Diao et al. 2004), which can be approximated at $\vartheta = \pi/2$. The variable v_{th} is the effective heat transport velocity and u is the integration variable. The thermal conductivity λ is taken from laboratory measurements (see Sect. "Calculation of the specific heat load"). Since the MILS also applies for steady-state conditions, in contrast to the ILS the later time data can be also evaluated. The parameter estimation problem is solved by minimising the root mean squared error (RMSE) by fitting R_{th} and v_{th} with the Nelder-Mead algorithm.

The Darcy velocity v_f can be calculated using the effective heat transport velocity (v_{th}) as follows (Zubair and Chaudhry 1996; Diao et al. 2004):

$$v_f = \frac{v_{th}\rho c_s}{\rho c_{p,w}} \tag{15}$$

ρc_s is the volumetric heat capacity of the soil.

Results and discussion

Averaging the specific heat load

The specific heat load, calculated using Eq. 3, is plotted in Fig. 2 about the heating time.

At the start of the heating, the specific heat load equals 22.8 W m^{-1} . This value is representative of the specific heat load assuming constant electrical resistance of the heating cable with time $q_{R=fix}$ (Table 2). Within the first minutes of heating, the specific heat load shows a strong decrease of nearly 10%. Then, the specific heat load varies between 20.5 W m^{-1} and 21.4 W m^{-1} with a time-averaged specific heat load of $q_{ave} = 20.8 \text{ W m}^{-1}$ (Table 2). Hence, the results show that although a constant voltage is applied to the heating cables, the specific heat load shows some variations during the ETRT, which are most significant at the start of the test. Thus, assuming constant electrical resistance can

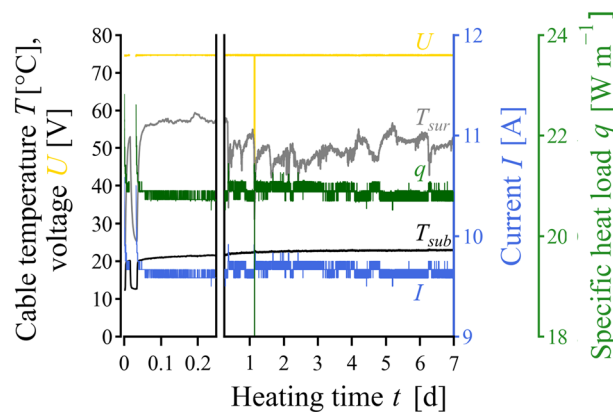


Fig. 2 Average cable temperatures at the surface (T_{sur}) and subsurface (T_{sub}), voltage (U), current (I) and specific heat load (q) during the heating time (t)

Table 2 Specific heat load (q), effective thermal conductivity (λ_{eff}), Darcy velocity (v_f) and hydraulic conductivity (k) for the different approaches of heat load determination: $q_{R=\text{fix}}$ assuming constant electrical resistance, average q_{ave} and adjusted q_{adj}

Specific heat load	q [W m ⁻¹]	λ_{eff} [W m ⁻¹ K ⁻¹]	v_f [m d ⁻¹] ^a	$k \times 10^{-3}$ [m s ⁻¹] ^b
$q_{R=\text{fix}}$	22.8 (± 0.8)	5.1 (± 0.2)	0.68 (± 0.18)	3.9 (± 1.0)
q_{ave}	20.9 (± 0.8)	4.6 (± 0.2)	0.57 (± 0.16)	3.2 (± 0.9)
q_{adj}	20.2 (± 1.1)	4.5 (± 0.2)	0.53 (± 0.15)	3.1 (± 0.9)

Measurement uncertainties are provided in brackets. The averages of depth-specific values are calculated by applying the arithmetic mean

^a From Péclet number analysis

^b From v_f assuming a constant hydraulic gradient of $i = 0.002$

account for an inaccuracy in the determination of the specific heat load. An average specific heat load is more representative of the heat load applied during the ETRT.

The change in the specific heat load during the ETRT can be explained by a change in the electrical resistance of the heating cable. The electrical current is a direct indicator of the electrical resistance as an integral value for the total cable length (Fig. 2). The change in the electrical resistance is a consequence of the change in the cable temperature. In Fig. 2, the average subsurface temperature T_{sub} and the average surface temperature T_{sur} are plotted complementary by calculating the arithmetic mean of the respective cable lengths. The temperature change and thus the change of the specific heat load is most distinct within the first minutes of the ETRT. The temperatures increase by around 11 K in the subsurface and by around 28 K at the surface. This first heating phase is attributed to the cable material, mainly the cable isolation (Fig. 1d). The variation of the specific heat load for the rest of the heating time can be attributed mainly to the part of the cable outside the borehole. At the surface, high diurnal temperature variations can be observed during the test. In the subsurface, these variations are considerably smaller. Hence, a depth-specific assessment of the specific heat load is suggested (Sect. "Spatial adjustment of the specific heat load").

Summarised, the assumption of constant electrical resistance is inappropriate for the calculation of the specific heat load. Prior knowledge of the cable's electrical resistance is insufficient to derive the heat load from the applied voltage. Further measurements of the heat load during the experiment are, therefore, necessary. Then, an average value can be calculated for the entire heating time. At the same time, the model assumption of constant heat load during the ETRT for effective thermal conductivity estimation can be confirmed. The average specific heat load is more representative of the heat load applied during the ETRT.

Spatial adjustment of the specific heat load

The theory of temperature-dependent resistances for adjusting the specific heat load along the depth of the BHE (Eq. 6) is applied. The results are plotted in Fig. 3. The specific heat loads along the entire length of the heating cable range between 20.2 W m⁻¹ and 23.0 W m⁻¹ (Fig. 3b). Higher specific heat loads can be found at the surface, whereas lower specific heat loads are calculated for the installed cable in the ground. According to the theory (Eq. 6), these differences are associated with the differences in the

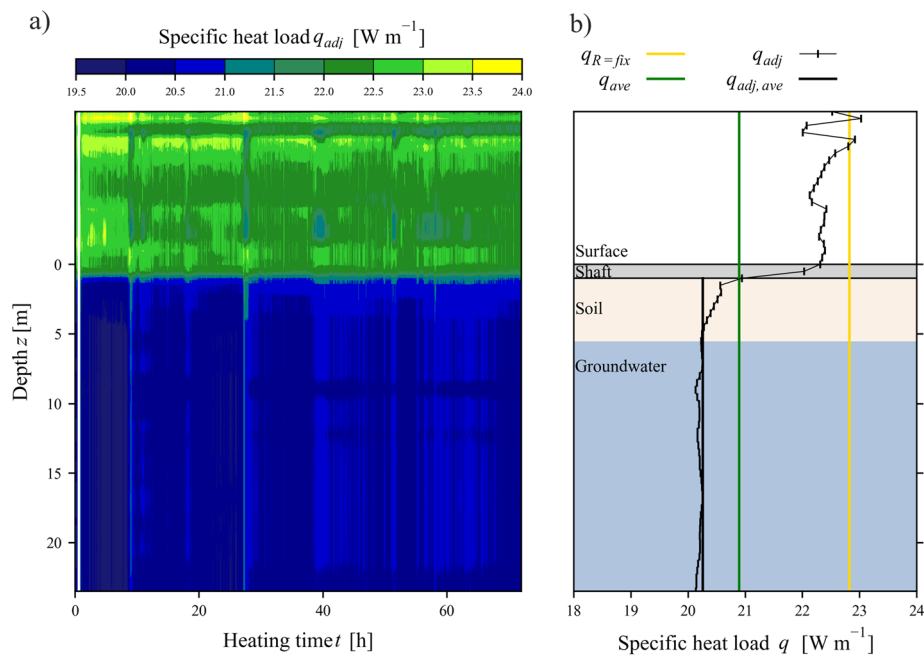


Fig. 3 Adjusted specific heat loads (q_{adj}) about the cable length: **a** plotted for the first 72 h of the ETRT, **b** averaged for the entire heating time in comparison with the specific heat load assuming constant electrical resistance ($q_{R=fix}$), the average specific heat load (q_{ave}) and the adjusted specific heat load averaged over depth ($q_{adj,ave}$)

temperature increase along the cable. The different temperature increases along the cable are associated with varying heat transport along the length of the cable.

Along the heating cable, three representative areas are identified: (1) The upper part of the heating cable is installed above the surface. Here, heat transfer is mainly characterised by the surrounding air and is expected to be low. Thus, the cable significantly heats up. Due to the diurnal temperature changes, high variations of the specific heat load during the heating time can be observed (Fig. 3a), which can also be seen in Fig. 2. (2) The lower part of the heating cable is installed below the groundwater level. Here, the heat transfer is characterised by conductive and convective transport and is expected to be quite good. Hence, the cable shows a low-temperature increase only due to the applied heat load. Compared to the upper part of the heating cable, only a marginal time dependency of the specific heat load is apparent. (3) Above the groundwater level, the heating cable is installed some meters in the vadose zone. Heat transfer is predominantly characterised by conduction. Moisture content and seepage can have an influence. Effectively, only the part of the heating cable installed inside the BHE can inject heat into the subsurface. Along the length of the heating cable inside the BHE, the heat load only varies within 3% between 20.2 and 20.6 W m^{-1} . Calculating the average of the adjusted specific heat loads for this part provides an average adjusted specific heat load of 20.2 W m^{-1} (Table 2). Figure 3b compares this value with the other approaches for heat load calculation (see Sect. "Averaging the specific heat load": $q_{R=fix}$ and $q_{adj,ave}$). The deviations between $q_{R=fix}$ and $q_{adj,ave}$ is 12% and only 3% between q_{ave} and $q_{adj,ave}$.

In this study, the variations along the depth of the BHE are minor. Overall, the variations of the specific heat along the cable length mainly depend on the following aspects:

(1) It is influenced by the material of the heating cable. The dependence of the electrical resistance and, therefore, of the specific heat load on the temperature is proportional to the temperature coefficient of resistance (TCR) of the material (Eq. 4). (2) The influence of the surface depends on the ambient conditions as well as the percentage of the heating cable above the surface, which is most often determined by the site-specific conditions. In this study, the ETRT was conducted in summertime with ambient temperatures above 28 °C during the day. The hybrid cable was exposed to the subsurface with a length of 24 m, which corresponds to 35% of the total cable length. (3) The heat transport in the subsurface determines the variation of the specific heat load along the depth of the BHE. When the thermal properties of the subsurface are very different along the depth, e.g., at a study site, where alternating layers of aquifers and aquitards are present, the temperature increase during the ETRT can vary considerably (> 30 K) with depth. This can account for a significant difference (> 8%) in the heat load at the different depths. Further information on the thermal properties of the subsurface in this study can be found in the following section.

Figure 3b emphasises that by adjusting the heat loads with the DTS measurements, the variation of the specific heat loads along the heating cable can be calculated. This method can be easily integrated into the evaluation procedure and is, therefore, highly recommended for the evaluation of future ETRTs. However, the application of this adjustment is limited to ETRT using hybrid cables or cables, where the fibre optic is in direct contact with the heating cable. Only then, the DTS temperature measurements can be used representatively for the temperature of the heating cable.

Depth-specific effective thermal conductivity evaluation

Table 2 summarises the depth-averaged results for the effective thermal conductivities, Darcy velocities and hydraulic conductivities applying different specific heat loads. The deviation in the effective thermal conductivity is proportional to the deviation in the specific heat load (Eq. 8). Thus, the errors of 3% and 12%, respectively, can also be found in this comparison. Referring to the results of Sects. "Averaging the specific heat load" and "Spatial adjustment of the specific heat load", the further discussion of the results focuses solely on the evaluation of applying the adjusted specific heat load.

With the ILS, the depth-averaged effective thermal conductivity is evaluated to $4.5 \text{ W m}^{-1} \text{ K}^{-1}$. With Péclet number analysis, an average Darcy velocity of 0.53 m d^{-1} is evaluated. Applying a hydraulic gradient of $i = 0.002$, an average hydraulic conductivity of $3.1 \times 10^{-3} \text{ m s}^{-1}$ is calculated. With the MILS an average Darcy velocity of 0.23 m d^{-1} is evaluated. The average hydraulic conductivity value analysed with the MILS is estimated to be $1.4 \times 10^{-3} \text{ m s}^{-1}$. Thereby, both hydraulic conductivity values are within the same order of magnitude as derived with the pumping test (k_{pt}) with $3.1 \times 10^{-3} \text{ m s}^{-1}$ (Reuß et al. 2012). Thus, the comparison between the different methods indicates that the evaluation of the ETRT regarding average Darcy velocity and hydraulic conductivity is successfully conducted (Table 2).

Over the entire depth of the BHE, heterogeneous thermal properties of the subsurface can be observed (Fig. 4).

The effective thermal conductivities vary between 1.9 and $9.3 \text{ W m}^{-1} \text{ K}^{-1}$ (Fig. 4b). Lower effective thermal conductivities are evaluated for the upper part of the borehole

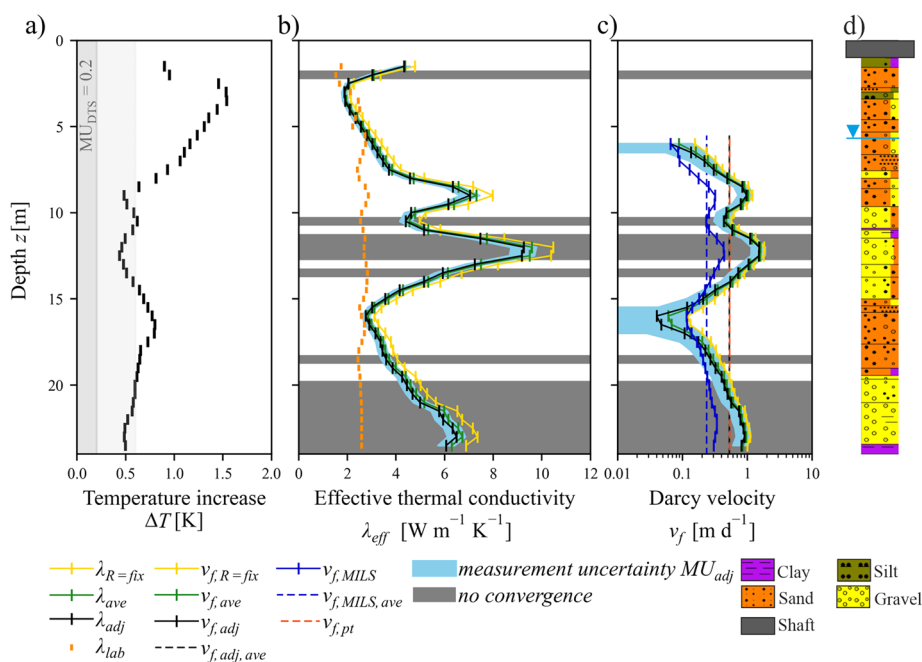


Fig. 4 Depth-specific results for **a** the representative transient temperature increase (ΔT), **b** the effective thermal conductivity (λ_{eff}) and **c** Darcy velocity (v_f) from the Péclet number analysis applying the different specific heat loads, and **d** the borehole profile. Darcy velocities are compared with results from the MILS analyses ($v_{f,\text{MILS}}$) and the pumping test ($v_{f,\text{pt}}$) by Reuß et al. (2012). Depth intervals where no convergence criterion ($\Delta\lambda_{\text{eff}}/\lambda_{\text{eff}} < 0.05/20 \text{ h}$) is obtained are highlighted in grey (i.e., no convergence)

and between 15.5 and 18 m. High effective thermal conductivities with values above $6 \text{ W m}^{-1} \text{ K}^{-1}$ are evaluated for depths around 9.5, 12.5 and 22 m. According to the results of the Péclet number analysis, these high effective thermal conductivities can be attributed to high Darcy velocities in the order of about $>0.6 \text{ m d}^{-1}$ and, therefore, to high hydraulic conductivities. The MILS results confirm areas of higher Darcy velocity (Fig. 4c), however, also indicate that high Darcy velocities are slightly overestimated with Péclet number analysis. Comparing the results with the borehole profile (Fig. 4d), elevated effective thermal conductivities and Darcy velocities correlate with zones of coarser sediments. In addition, the evaluated hydraulic conductivities are between 1.1×10^{-4} and $8.8 \times 10^{-3} \text{ m s}^{-1}$, which are in the range of typical sand and gravel aquifers (Domenico and Schwartz 1990).

Discussion

In the following paragraph limitations of this study are discussed. Figure 5 shows the evaluation procedure for effective thermal conductivity for two representative depth intervals (5 m and 12.5 m). Complementary, the evaluation of all 45 analysed depth intervals can be found in the supporting information (Additional file 1: Figs. S1–S45).

The depth interval at 5 m represents a conduction-dominated depth interval. The entire time data shows a transient temperature increase. Applying forward modelling, the effective thermal conductivity results converge to a stable value within the convergence criterion of $\Delta\lambda_{\text{eff}}/\lambda_{\text{eff}} < 0.05$ within 20 h. Contrary, the depth interval at 12.5 m is advection-dominated. The iterative evaluation indicates strong groundwater influences

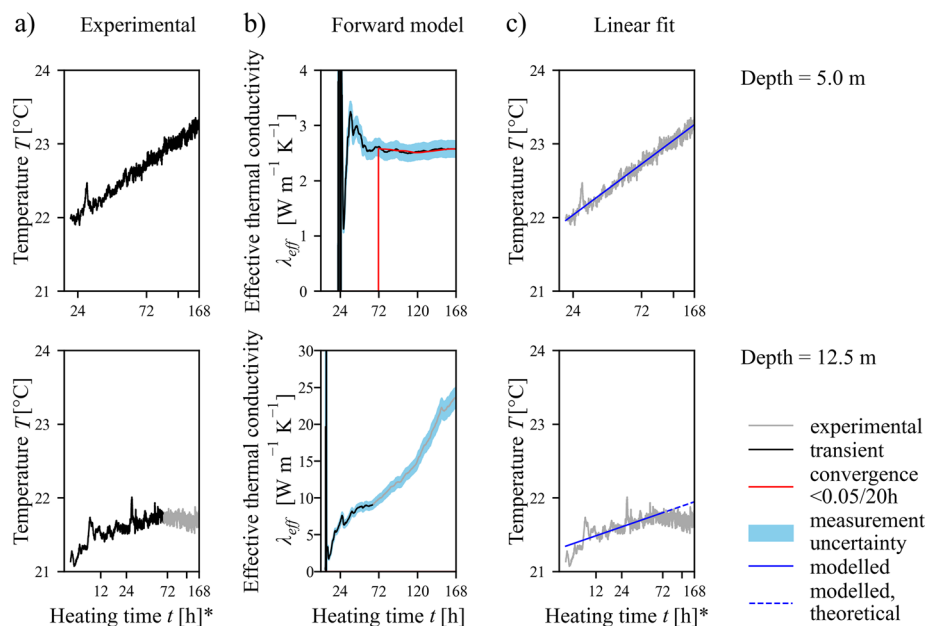


Fig. 5 Evaluation of the effective thermal conductivities (λ_{eff}) for two representative depths of 5.0 m and 12.5 m, respectively: **a** Identifying the transient temperature increase from the experimental data, **b** applying sequential forward evaluation with the ILS and testing for convergence of the result, **c** deriving parameters for linear fit. *Please note that the axes are scaled to the natural logarithm

showing an increase in effective thermal conductivities with evaluation time. The later temperature–time data approaches a steady state value and is not evaluated with ILS. Hence, no convergence is obtained. In Fig. 4, the areas, where convergence of the effective thermal conductivity result cannot be achieved are highlighted. Convergence cannot be achieved for 33% of the evaluated depth intervals, which are associated with high advective heat transport. In depth intervals with high groundwater flow, the system quickly approaches steady-state conditions, which reduces the evaluation time. For these depth intervals, near-steady-state conditions are achieved within 2–3 days. Hence, fewer data points can be used for linear regression. The degree of determination R^2 is lower (<0.85 , for $z = 12$ m and 12.5 m <0.7). Summarised, even though the ILS evaluation is conducted for all depth intervals, the assumptions of the ILS are invalid for some areas of high Darcy velocities. This is indicated by the convergence criterion and the overestimation of the Darcy velocities in comparison with the MILS.

In addition, the Péclet number analysis to estimate Darcy velocities from ILS results has to be examined critically. Applying the Péclet number analysis, several assumptions are made that contribute to the uncertainty of the estimate. (1) The method defines the advective heat flow component by the difference between effective thermal conductivity λ_{eff} and thermal conductivity by conduction only λ . However, whereas thermal conductivity λ increases linearly with the specific heat load (Eq. 7), the effective thermal conductivity at groundwater-influenced conditions increases non-linearly (Eq. 14). (2) The characteristic length is an ambiguous number. It depends on the experiment time and the heat transfer properties of the medium. By defining the characteristic length as a fixed value equal to the borehole radius, the estimated Darcy velocities are assumed to be defined mainly by the properties of the borehole. Thereby, a conservative calculation

approach is chosen, which can result in an overestimation of higher Darcy velocities. Instead of the borehole radius, the radius of temperature influence would be a more suitable value. However, the determination of this value is challenging. (3) Thermal conductivity values of the subsurface have to be known. In this study, thermal conductivities from laboratory measurements of disturbed samples are used. Thus, there are uncertainties, e.g., whether the depth-specific laboratory values actually represent the thermal conductivities at in-situ conditions or whether these values represent the considered soil volume influenced by the TRT. Alternatively, thermal conductivities can be defined from ETRT results influenced by conduction only, thereby, defining one single value of thermal conductivity for the entire depth of the BHE. As indicated in Fig. 4b, average deviations of 14% between the thermal conductivities from laboratory measurements and ETRT results can be observed (depth interval 2.5 to 5.5 m). Regarding these uncertainties, the Péclet analysis can only be used to give a rough estimate. For a more precise determination of Darcy velocities from ETRT results the MILS has to be applied. Nevertheless, with the ILS, valid estimates of the average values and qualitative identification of areas of enhanced heat transport are analysed. Despite a higher uncertainty of the results, the lower computational effort justifies the application of the ILS.

In depth intervals with high groundwater flow, the heat is transported fast away from the BHE. Thus, the temperature increase, that can be used for evaluation, is low (< 0.6 K, Fig. 4a). Overall, temperature fluctuations within the DTS data in the order of $\Delta T \sim 0.1$ K are observed. Thus, for depth intervals with a low-temperature increase, the uncertainty of the calculation increases, too. The applied specific heat load of 20 W m^{-1} for this highly advective aquifer does not generate a sufficient temperature increase to evaluate for all depths (Fig. 4a), however, is in the typical range of specific heat loads applied in TRT studies using heating cables between 6.1 to 48 W m^{-1} with an average of about 25 W m^{-1} (Freifeld et al. 2008; Raymond et al. 2010; Huber 2013; Lehr and Sass 2014; Vieira et al. 2017; Galgaro et al. 2018; Vélez Márquez et al. 2018; Maldaner et al. 2019; Zhang et al. 2020; Minchio et al. 2020; Antelmi et al. 2020; Giordano et al. 2021; Dalla Santa et al. 2022; Hakala et al. 2022; Simon and Bour 2022).

The duration of the ETRT within this study was about 170 h, which is quite long for a TRT. Concerning the evaluation of a TRT, the longer the testing time, the bigger the sample volume of the subsurface. Hence, the effect of the grouting material decreases with time, as well as the influence of inhomogeneity of the subsurface. Thus, a more representative evaluation of the subsurface conditions can be conducted, especially by combining it with the sequential forward modelling (Sect. "Evaluation of depth-specific effective thermal conductivities"). However, regarding the practical application of ETRT, a shorter test duration is required. From Additional file 1: Figs. S1–S45, a testing time of about 80 to 90 h can be recommended that allows for a clear identification of the turning point, when effective thermal conductivity values start to increase and, therefore, to evaluate the groundwater effect. Nevertheless, the required testing time depends on site-specific conditions, such as the subsurface conditions, the grouting material and the borehole radius.

Figure 6 shows the relation between Darcy velocities and effective thermal conductivities as evaluated in this study and compared to reported values from other studies dealing with the determination of groundwater flow velocities from TRT data from TRT

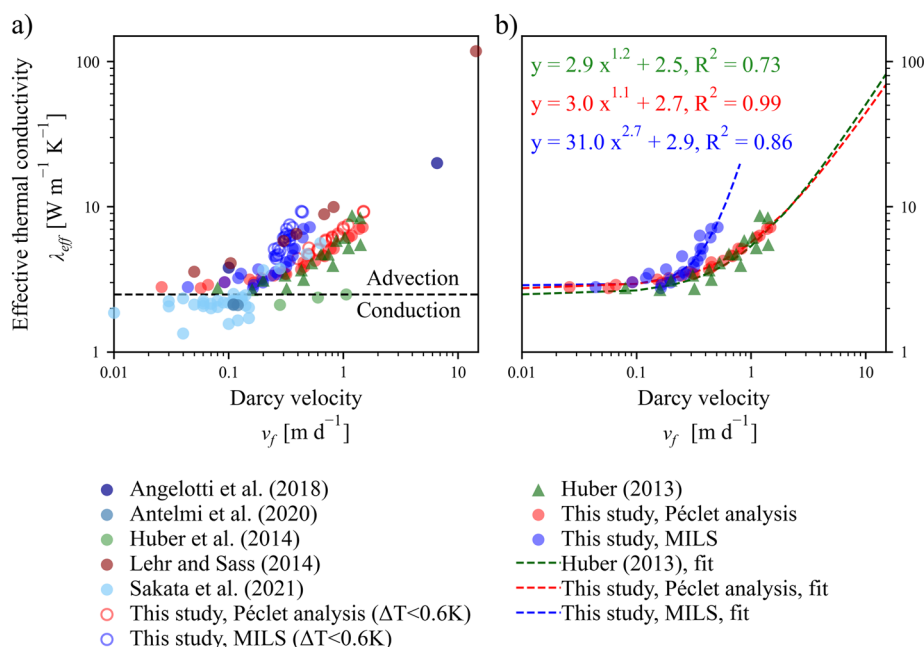


Fig. 6 Darcy velocities (v_f) and corresponding effective thermal conductivities (λ_{eff}) from studies evaluating groundwater-influenced TRTs, **a** all data sets, **b** data sets used for curve fitting. The colour code indicates the applied evaluation method (blue = MILS, red = Péclet number analysis, green = experimentally set Darcy velocity). The symbol code indicates the test method (circle = field study, triangle = sandbox experiment)

data (Angelotti et al. 2018, Antelmi et al. 2020, Huber 2013, Huber et al. 2014, Lehr and Sass 2014, Sakata et al. 2021).

It contains data from different aquifer types with varying properties. In addition, different TRT methods and evaluation procedures were applied. The data collection highlights that with increasing Darcy velocities, effective thermal conductivities also increase. In Fig. 6b, the correlation between these two properties is separately fitted for three distinct data sets, including the two data sets from this study and the data set from Huber (2013), where Darcy velocities were experimentally set in sandbox experiments. The power function in the form of $y = ax^b + c$ is fitted to the data. If the exponent b becomes 1.0 the power function will take the form of a linear equation. Thus, comparison of linear and exponentiating relationship between the Darcy velocity and effective thermal conductivities is made easier. The parameter c corresponds to the thermal conductivity λ without groundwater flow. Thus, it depends highly on the geologic conditions of the study site. The average thermal conductivity of this study determined in the laboratory is $2.5 \text{ W m}^{-1} \text{ K}^{-1}$. The deviations of c from this value also indicate the difficulty in distinguishing between the heat transport mechanism of conduction and advection at low flow conditions. The relationship in Fig. 6b shows that effective thermal conductivity is not significantly affected by groundwater flow up to a Darcy flow of about 0.2 to 0.3 m d^{-1} . With increasing Darcy velocities, the effective thermal conductivity increases significantly. The highest degree of determination is achieved for the results of the Péclet number analysis. This is expected, as the Darcy velocities are directly derived from the effective thermal conductivities based on a linear relationship (Eq. 12). The deviation from the perfect correlation is mainly due to the variance in thermal

conductivity derived from laboratory measurements. However, the assumptions made for the evaluation with the Péclet number analysis result in high uncertainties in the estimation of Darcy velocities with this method, as discussed before in detail. The data set with the lowest degree of determination is the data set from Huber (2013), which can be easily explained. On one hand, different measurement methods were applied. The effective thermal conductivities are evaluated from temperature–time data, whereas the Darcy velocities are measured with flowmeters. On the other hand, results from several tests are combined in one data set. The fit calculated for the data set by Huber (2013) agrees well with the fit for the Péclet number analysis, which supports the assumptions made for the Péclet number analysis. However, it does not prove that the Péclet number analysis is the recommended analysis method for this specific case study.

The MILS fit significantly deviates from the best fit of the other two data sets. The plotted MILS data set includes the results of both evaluation methods (ILS and MILS) based on the same experimental data (Fig. 6). Although, the chosen convergence criterion was acceptable for evaluation using the ILS. The latter is not the recommended model for the evaluation of groundwater-influenced TRT. However, uncertainties, therefore, still remain, which could result in an overestimation of the derived effective thermal conductivities especially for higher Darcy velocities. To address these uncertainties during the evaluation of ETRTs, we recommend performing field experiments under controlled groundwater flow velocities combined with numerical heat transport models.

For the conduct of future ETRTs with high groundwater influence, the knowledge derived from this study can provide valuable insights. Ensuring a sufficient temperature increase for the evaluation of all depth intervals is crucial for the reliable determination of effective thermal conductivities and groundwater velocities. This could reduce the sensitivity of the data towards temperature noise and at the same time improve the estimation of the regression (Fig. 6) and, therefore, of the depth-specific effective thermal conductivities. Nevertheless, increasing the specific heat load for ETRT is not trivial. Depending on the experimental setup and conduct, different aspects have to be considered. In principle, it applies, that the higher the heat load, the higher the temperature increase. However, the highest possible heat load is defined by cable specifications. Typically, the maximum temperature allowed for such cables is 60 to 80 °C. Especially in the upper part of the heating cable, when the cable is in contact with air, there is a high risk of overheating at high specific heat loads (Fig. 2). Hence, to increase the heat load during the ETRT, the heat transfer in the surface area has to be improved. Thus, actions against overheating are necessary, e.g., burying the cable or placing water-filled tubes on it. In the study by Hakala et al. (2022), they used an air fan to cool the cable. However, practical issues and site characteristics, such as the duration of the experiment, the available space to bury the cable, and the necessary length of the cable above the surface have to be considered. Apart from that, improvements in the material of the heating cable towards the application at elevated temperatures are desirable. A compromise between decreasing the thermal resistance of the heating cable, and at the same time maintaining sufficient electrical isolation when working with current in a wet environment have to be made. In addition, the fibre optics have to be protected against moisture. Otherwise, the temperature measurement becomes inaccurate. Further issues applying a higher heat

load have to be considered. For ETRTs in open boreholes or with the heating cable installed inside the heat exchanger pipe induced convection can occur. Regarding this, Hakala et al. (2022) recommended a maximum specific heat load of 20 W m^{-1} . However, a grouted cable is used in this study indicating a minor influence. There are only a few studies, which compare the influence of the heat load on the results of TRTs. Huber (2013), for example, compared in his ETRT study different specific heat loads at the same BHE ranging from 6 to 46 W m^{-1} . He observed that less variation in depth-specific thermal conductivities was resolved by applying a higher specific heat load. Partly, this could be explained by a lower influence on the accuracy of the temperature measurement due to a higher temperature increase. In addition to increase the heat load, the uncertainty of the slope can be reduced using temperature measurements with better accuracy than DTS. This includes placing additional punctual temperature sensors or combining DTS data with temperature profiles from wireless measurement tools (Schüppler et al. 2021).

Conclusion

In this study, an ETRT is evaluated with significant groundwater flow ($>0.2 \text{ m d}^{-1}$). Different approaches for the determination of the specific heat load of the ETRT are discussed. Evaluations of effective thermal conductivities and Darcy velocities are conducted by applying the ILS combined with the Péclet number analysis and the MILS. Depth-averaged effective thermal conductivity and hydraulic conductivity are evaluated to be $4.5 \text{ W m}^{-1} \text{ K}^{-1}$ and $3.1 \times 10^{-3} \text{ m s}^{-1}$, respectively. Considering the results of this study, the following conclusions can be made:

- (1) Assuming constant electrical resistance of the heating cable can account for an inaccuracy of 12% in the determination of depth-specific effective thermal conductivities. Thus, this method is inappropriate for the calculation of the specific heat load. Hence, time-averaging of the heat load by logging voltage and current during the ETRT is recommended.
- (2) Applying the theory of temperature-dependent resistances, the variation of the specific heat loads along the length of the heating cable can be adjusted. In this study, variations within 3% were observed along the BHE. For hydrogeological conditions with varying groundwater flow (i.e., at a study site with alternating layers of aquifers and aquitards), the variations are expected to be more significant. The adjustment of the specific heat loads can be easily integrated into the evaluation procedure and is, therefore, also recommended.
- (3) For high Darcy velocities, experimental issues ensuring a sufficient temperature increase ($\Delta T > 0.6 \text{ K}$) are shown to increase the uncertainty of the evaluation. To reduce the sensitivity towards temperature fluctuations, measures applying a higher specific heat load are desirable. This includes actions against overheating of the cable outside the borehole heat exchanger and improvements of the material of the heating cable towards the application at elevated temperatures ($> 60 \text{ }^\circ\text{C}$). In 33% of the analysed depth intervals, due to a fast adjustment of the system to the applied heat load, the convergence criterion of $\Delta\lambda_{\text{eff}}/\lambda_{\text{eff}} < 0.05/20 \text{ h}$ of the ILS sequential

forward evaluation cannot be achieved. Temperature measurements with better accuracy (adding punctual sensors, in combination with profiles from wireless measurement tools) are expected to also improve the evaluation of ETRT.

Finally, to address the uncertainties during the evaluation of ETRTs with high groundwater flow, we recommend performing field experiments under controlled groundwater flow velocities combined with numerical heat transport models.

List of symbols

Latin symbols

A	Cross-sectional area [m^2]
A-DTS	Active distributed temperature sensing
ATRT	Actively heated fibre optic thermal response test
bgl	Below ground level
BHE	Borehole heat exchanger
DTRT	Distributed thermal response test
DTS	Distributed temperature sensing
E_i	Exponential integral
ETRT	Enhanced thermal response test
GSHHP	Ground source heat pump
i	Hydraulic gradient
I	Current [A]
ILS	Infinite line source model
k	Hydraulic conductivity [m s^{-1}]
l	Cable length [m]
l_c	Characteristic length [m]
m	Slope [K ln(s)^{-1}]
MILS	Moving infinite line source model
Pe	Péclet number
PE	Polyethylene
P_{el}	Electrical power [W]
Q	Heat load [W]
q	Specific heat load [W m^{-1}]
q_{adj}	Adjusted specific heat load [W m^{-1}]
q_{ave}	Average specific heat load [W m^{-1}]
$q_{R=fix}$	Specific heat load assuming constant electrical resistance [W m^{-1}]
R	Electrical resistance [Ω]
R^2	Degree of determination
r	Distance [m]
r_b	Borehole radius [m]
R_T	Electrical resistance at a defined temperature [Ω]
R_{T20}	Reference electrical resistance [Ω]
R_{th}	Thermal borehole resistance [m K W^{-1}]
T	Temperature [$^{\circ}\text{C}$]
T_{sub}	Subsurface temperature [$^{\circ}\text{C}$]
T_{sur}	Surface temperature [$^{\circ}\text{C}$]
t	Time [s]
T_0	Reference temperature [$^{\circ}\text{C}$]
TCR	Temperature coefficient of resistance
TRT	Thermal response test
u	Integration variable
U	Voltage [V]
VDI	Verein Deutscher Ingenieure
v_f	Darcy velocity [m d^{-1}]
v_{th}	Effective heat transport velocity [m s^{-1}]
z	Depth [m]

Greek symbols

α	Thermal diffusivity [$\text{m}^2 \text{s}^{-1}$]
α_{T20}	Temperature coefficient of resistance [K^{-1}]
γ	Euler's constant
ϑ	Angle to the groundwater flow direction
λ	Thermal conductivity [$\text{W m}^{-1} \text{K}^{-1}$]

λ_{eff}	Effective thermal conductivity [$\text{W m}^{-1} \text{K}^{-1}$]
ρC_s	Volumetric heat capacity of the soil [$\text{J m}^{-3} \text{K}^{-1}$]
ρC_w	Volumetric heat capacity of water [$\text{J m}^{-3} \text{K}^{-1}$]
ρ_{T20}	Reference resistivity [$\Omega \text{mm}^2 \text{m}^{-1}$]

Supplementary Information

The online version contains supplementary material available at <https://doi.org/10.1186/s40517-023-00278-y>.

Additional file 1. Evaluation of effective thermal conductivities with the infinite line source model for all evaluated depth-intervals.

Acknowledgements

The authors would like to thank Andreas Köhler of the Biberach University of Applied Sciences for his help with the ETRT measurements and provision of the Pt100 temperature data. The helpful comments of the two reviewers are also gratefully acknowledged.

Author contributions

AA, HS and PB developed the methodology and designed the study. AA, HS and RZ carried out the TRT. AA executed the data analysis and prepared the draft of the manuscript. All authors read and approved the final manuscript.

Funding

Open Access funding enabled and organized by Projekt DEAL. This study was funded by the funding programme QEWS-plus (Grant Number 03EE4020B, 03EE4020E, <https://www.qewsplus.de/>) by the Federal Ministry for Economic Affairs and Climate Action.

Availability of data and materials

The data sets used and/or analysed during the current study are available from the corresponding author upon reasonable request.

Declarations

Competing interests

The authors declare that they have no competing interests.

Received: 4 October 2023 Accepted: 4 December 2023

Published online: 03 January 2024

References

- Acuña J. Distributed thermal response tests—new insights on U-pipe and Coaxial heat exchangers in groundwater-filled boreholes [Dissertation]. Stockholm: KTH Royal Institute of Technology; 2013.
- Angelotti A, Ly F, Zille A. On the applicability of the moving line source theory to thermal response test under groundwater flow: considerations from real case studies. *Geothermal Energy*. 2018. <https://doi.org/10.1186/s40517-018-0098-z>.
- Antelmi M, Alberti L, Angelotti A, Curnis S, Zille A, Colombo L. Thermal and hydrogeological aquifers characterization by coupling depth-resolved thermal response test with moving line source analysis. *Energy Convers Manage*. 2020. <https://doi.org/10.1016/j.enconman.2020.113400>.
- Bakker M, Caljé R, Schaars F, van der Made K-J, de Haas S. An active heat tracer experiment to determine groundwater velocities using fiber optic cables installed with direct push equipment. *Water Resour Res*. 2015;51(4):2760–72. <https://doi.org/10.1002/2014WR016632>.
- Banks EW, Shanafield MA, Cook PG. Induced temperature gradients to examine groundwater flowpaths in open boreholes. *Groundwater*. 2014;52(6):943–51. <https://doi.org/10.1111/gwat.12157>.
- Bense VF, Read T, Bour O, Le Borgne T, Coleman T, Krause S, et al. Distributed temperature sensing as a downhole tool in hydrogeology. *Water Resour Res*. 2016;52(12):9259–73. <https://doi.org/10.1002/2016WR018869>.
- Bussmann G, Bracke R, Eicker T, Wittig V, Tuente H, Gueldenhaupt J, et al. GeoStar—a scalable borehole heat exchanger plant for growing district heating systems and restricted urban areas. In: *World Geothermal Congress*; 19–25 April; Melbourne, Australia; 2015.
- Carslaw HS, Jaeger JC. *Conduction of heat in solids*. 2nd ed. Oxford: Oxford Science Publications; 1959.
- Chiasson A, Rees SJ, Spittler JD. A preliminary assessment of the effects of groundwater flow on closed-loop ground-source heat pump systems. *ASHRAE Trans*. 2000;106:380–93.
- Ciocca F, Lunati I, van de Giesen N, Parlange MB. Heated optical fiber for distributed soil-moisture measurements: a lysimeter experiment. *Vadose Zone J*. 2012. <https://doi.org/10.2136/vzj2011.0199>.
- Coleman TI, Parker BL, Maldaner CH, Mondanos MJ. Groundwater flow characterization in a fractured bedrock aquifer using active DTS tests in sealed boreholes. *J Hydrol*. 2015;528:449–62. <https://doi.org/10.1016/j.jhydrol.2015.06.061>.
- Dalla Santa G, Pasquier P, Schenato L, Galgaro A. Repeated ETRTs in a complex stratified geological setting: high-resolution thermal conductivity identification by multiple linear regression. *J Geotech Geoenviron Eng*. 2022. [https://doi.org/10.1061/\(ASCE\)GT.1943-5606.0002724](https://doi.org/10.1061/(ASCE)GT.1943-5606.0002724).

- Del Val L, Carrera J, Pool M, Martínez L, Casanovas C, Bour O, Folch A. Heat dissipation test with fiber-optic distributed temperature sensing to estimate groundwater flux. *Water Resour Res.* 2021. <https://doi.org/10.1029/2020WR027228>.
- Des Tombe BF, Bakker M, Smits F, Schaars F, van der Made K-J. Estimation of the variation in specific discharge over large depth using distributed temperature sensing (DTS) measurements of the heat pulse response. *Water Resour Res.* 2019;55(1):811–26. <https://doi.org/10.1029/2018WR024171>.
- Diao N, Li Q, Fang Z. Heat transfer in ground heat exchangers with groundwater advection. *Int J Therm Sci.* 2004;43(12):1203–11. <https://doi.org/10.1016/j.ijthermalsci.2004.04.009>.
- Domenico PA, Schwartz FW. *Physical and chemical hydrogeology*. Hoboken: John Wiley & Sons, Inc.; 1990.
- Ferguson G. Screening for heat transport by groundwater in closed geothermal systems. *Groundwater.* 2015;53(3):503–6. <https://doi.org/10.1111/gwat.12162>.
- Freifeld BM, Finsterle S, Onstott TC, Toole P, Pratt LM. Ground surface temperature reconstructions: using in situ estimates for thermal conductivity acquired with a fiber-optic distributed thermal perturbation sensor. *Geophys Res Lett.* 2008. <https://doi.org/10.1029/2008GL034762>.
- Fujii H, Okubo H, Itoi R. Thermal response tests using optical fiber thermometers. *GRC Trans.* 2006;30:559–63.
- Galgaro A, Pasquier P, Schenato L, Cultrera M, Santa GD. Soil thermal conductivity from early TRT logs using an active hybrid optic fibre system. 2018:1–9. <https://doi.org/10.22488/okstate.18.000023>.
- Gehlin S. Thermal response test: method development and evaluation [Dissertation]. Luleå: Luleå University of Technology; 2002.
- Giordano N, Lamarche L, Raymond J. Evaluation of subsurface heat capacity through oscillatory thermal response tests. *Energies.* 2021;14(18):5791. <https://doi.org/10.3390/en14185791>.
- Hacker V, Sumereder C. *Electrical engineering: fundamentals*. München, Wien: De Gruyter Oldenbourg; 2020.
- Hakala P, Vallin S, Arola T, Martinkauppi I. Novel use of the enhanced thermal response test in crystalline bedrock. *Renew Energy.* 2022. <https://doi.org/10.1016/j.renene.2021.10.020>.
- Heske C, Kohlsch O, Dornstädter J, Heidinger P. Der Enhanced-Geothermal-Response-Test als Auslegunggrundlage und Optimierungstool. *bbr Sonderheft.* 2011.
- Huber H. Experimentelle und numerische Untersuchungen zum Wärmetransportverhalten oberflächennaher, durchströmter Böden [Dissertation]. Darmstadt: Technical University of Darmstadt; 2013.
- Huber H, Arslan U, Sass I. Zum Einfluss der Filtergeschwindigkeit des Grundwassers auf die effektive Wärmeleitfähigkeit. *Grundwasser.* 2014;19(3):173–9. <https://doi.org/10.1007/s00767-014-0263-7>.
- Katsura T, Nagano K, Takeda S, Shimakura K. Heat transfer experiment in the ground with groundwater advection. In: The IEA 10th Energy Conservation Thermal Energy Storage Conference. New Jersey, USA; 2006.
- Kuchling H. *Taschenbuch der Physik*. 21st ed. München: Carl Hanser verlag GmbH & Co. KG; 2014.
- Lehr C, Sass I. Thermo-optical parameter acquisition and characterization of geologic properties: a 400-m deep BHE in a karstic alpine marble aquifer. *Environ Earth Sci.* 2014;72(5):1403–19. <https://doi.org/10.1007/s12665-014-3310-x>.
- Luo J, Rohn J, Xiang W, Bayer M, Priess A, Wilkmann L, et al. Experimental investigation of a borehole field by enhanced geothermal response test and numerical analysis of performance of the borehole heat exchangers. *Energy.* 2015;84:473–84. <https://doi.org/10.1016/j.energy.2015.03.013>.
- Maldaner CH, Munn JD, Coleman TI, Molson JW, Parker BL. Groundwater flow quantification in fractured rock boreholes using active distributed temperature sensing under natural gradient conditions. *Water Resour Res.* 2019;55(4):3285–306. <https://doi.org/10.1029/2018WR024319>.
- Meschede D. *Gerthsen Physik*. 25th ed. Berlin, Heidelberg: Springer Spektrum; 2015.
- Minchio F, Cesari G, Pastore C, Fossa M. Experimental hydration temperature increase in borehole heat exchangers during thermal response tests for geothermal heat pump design. *Energies.* 2020;13(13):3461. <https://doi.org/10.3390/en13133461>.
- Molina-Giraldo N, Bayer P, Blum P. Evaluating the influence of thermal dispersion on temperature plumes from geothermal systems using analytical solutions. *Int J Therm Sci.* 2011;50(7):1223–31. <https://doi.org/10.1016/j.ijthermalsci.2011.02.004>.
- Pambou CHK, Raymond J, Lamarche L. Improving thermal response tests with wireline temperature logs to evaluate ground thermal conductivity profiles and groundwater fluxes. *Heat Mass Transfer.* 2019;55(6):1829–43. <https://doi.org/10.1007/s00231-018-2532-y>.
- Raymond J, Robert G, Therrien R, Gosselin L. A novel thermal response test using heating cables. In: *World Geothermal Congress; 25–29 April; Bali, Indonesia; 2010*.
- Read T, Bour O, Selker JS, Bense VF, Le Borgne T, Hochreutener R, Lavenant N. Active-distributed temperature sensing to continuously quantify vertical flow in boreholes. *Water Resour Res.* 2014;50(5):3706–13. <https://doi.org/10.1002/2014WR015273>.
- Reuß M, Koenigsdorff R, Zorn R, Kuckelkorn J, Steger H, Pröll M, Feuerstein P. Qualitätssicherung bei Erdwärmesonden und Erdreichkollektoren, Final report, Federal Ministry for Economic Affairs and Technology (FKZ: 0327453A). 2012.
- Riegger M, Heidinger P, Lorinser B, Stober I. Auswerteverfahren zur Kontrolle der Verfüllqualität in Erdwärmesonden mit faseroptischen Temperaturmessungen. *Grundwasser.* 2012;17(2):91–103. <https://doi.org/10.1007/s00767-012-0192-2>.
- Sakata Y, Katsura T, Serageldin AA, Nagano K, Ooe M. Evaluating variability of ground thermal conductivity within a steep site by history matching underground distributed temperatures from thermal response tests. *Energies.* 2021;14(7):1872. <https://doi.org/10.3390/en14071872>.
- Sanner B, Hellström G, Spitler J, Gehlin S. Thermal response test—current status and world-wide application. In: *World Geothermal Congress; 24–29 April; Antalya, Turkey; 2005*.
- Sayde C, Buelga JB, Rodriguez-Sinobas L, El Khoury L, English M, van de Giesen N, Selker JS. Mapping variability of soil water content and flux across 1–1000 m scales using the Actively Heated Fiber Optic method. *Water Resour Res.* 2014;50(9):7302–17. <https://doi.org/10.1002/2013WR014983>.
- Schüppler S, Zorn R, Steger H, Blum P. Uncertainty analysis of wireless temperature measurement (WTM) in borehole heat exchangers. *Geothermics.* 2021;90:102019. <https://doi.org/10.1016/j.geothermics.2020.102019>.

- Signorelli S, Bassetti S, Pahud D, Kohl T. Numerical evaluation of thermal response tests. *Geothermics*. 2007;36(2):141–66. <https://doi.org/10.1016/j.geothermics.2006.10.006>.
- Simon N, Bour O. An ADTS toolbox for automatically interpreting active distributed temperature sensing measurements. *Ground Water*. 2022. <https://doi.org/10.1111/gwat.13172>.
- Spitler JD, Gehlin SE. Thermal response testing for ground source heat pump systems—an historical review. *Renew Sustain Energy Rev*. 2015;50:1125–37. <https://doi.org/10.1016/j.rser.2015.05.061>.
- Stauffer F, Bayer P, Blum P, Giraldo NM, Kinzelbach W. Thermal use of shallow groundwater. Boca Raton: CRC Press; 2014.
- Vélez Márquez M, Raymond J, Blessent D, Philippe M, Simon N, Bour O, Lamarche L. Distributed thermal response tests using a heating cable and fiber optic temperature sensing. *Energies*. 2018;11(11):3059. <https://doi.org/10.3390/en11113059>.
- Verein Deutscher Ingenieure. VDI 4640 part 1, Thermal use of the underground, Fundamentals, approvals, environmental aspects. 2010.
- Verein Deutscher Ingenieure. VDI 4640 part 5, Thermal use of the underground, Thermal response test (TRT). 2020.
- Vieira A, Alberdi-Pagola M, Christodoulides P, Javed S, Loveridge F, Nguyen F, et al. Characterisation of ground thermal and thermo-mechanical behaviour for shallow geothermal energy applications. *Energies*. 2017;10(12):2044. <https://doi.org/10.3390/en10122044>.
- Wagner V, Blum P, Kübert M, Bayer P. Analytical approach to groundwater-influenced thermal response tests of grouted borehole heat exchangers. *Geothermics*. 2013;46:22–31. <https://doi.org/10.1016/j.geothermics.2012.10.005>.
- Wilke S, Menberg K, Steger H, Blum P. Advanced thermal response tests: a review. *Renew Sustain Energy Rev*. 2020;119:109575. <https://doi.org/10.1016/j.rser.2019.109575>.
- Witte HJ. Error analysis of thermal response tests. *Appl Energy*. 2013;109:302–11. <https://doi.org/10.1016/j.apenergy.2012.11.060>.
- Zhang B, Gu K, Shi B, Liu C, Bayer P, Wei G, et al. Actively heated fiber optics based thermal response test: a field demonstration. *Renew Sustain Energy Rev*. 2020;134:110336. <https://doi.org/10.1016/j.rser.2020.110336>.
- Zhang X, Han Z, Ji Q, Zhang H, Li X. Thermal response tests for the identification of soil thermal parameters: a review. *Renew Energy*. 2021;173:1123–35. <https://doi.org/10.1016/j.renene.2020.12.028>.
- Zubair SM, Chaudhry MA. Temperature solutions due to time-dependent moving-line-heat sources. *Heat Mass Transf*. 1996;31(3):185–9. <https://doi.org/10.1007/s002310050044>.

Publisher's Note

Springer Nature remains neutral with regard to jurisdictional claims in published maps and institutional affiliations.

Submit your manuscript to a SpringerOpen[®] journal and benefit from:

- ▶ Convenient online submission
- ▶ Rigorous peer review
- ▶ Open access: articles freely available online
- ▶ High visibility within the field
- ▶ Retaining the copyright to your article

Submit your next manuscript at ▶ [springeropen.com](https://www.springeropen.com)
